Available online at www.sciencedirect.com
SCIENCE DIRECT®
Journal of Power Sources 141 (2005) 340–350
JOURNAL OF POWER SOURCES
www.elsevier.com/locate/jpowsour

Improved performance of rechargeable alkaline batteries via surfactant-mediated electrosynthesis of MnO_2

M. Ghaemi[a,*], L. Khosravi-Fard[a], J. Neshati[b]

[a] *Department of Chemistry, School of Sciences, Tarbiat Modarres University, P.O. Box 14115-175, Tehran 4838, Iran*
[b] *Department of Chemistry, K.N. Toosi University of Technology, Tehran, Iran*

Received 21 July 2004; received in revised form 6 October 2004; accepted 6 October 2004
Available online 18 November 2004

Abstract

An innovative application of surfactant-mediated modifications of electrolytic MnO_2 (EMD), proved to be a major step toward enhancement of the rechargeability in alkaline batteries. Presence of different surfactants in boiling acidic solutions of manganese sulfate, under atmospheric pressure, enhanced a variety of EMD products, with various structural and electrochemical properties. Surfactants employed consisted of: anionic sodium *n*-dodecylbenzenesulfonate (SDBS), cationic cetyltrimethylammonium bromide (CTAB) and non-ionic *t*-octyl phenoxy polyethoxyethanol (Triton X-100). Among them, EMDs produced in the presence of CTAB has a slight positive effect on the cycle performances, while SDBS inhibits it. Interestingly, the EMD powders prepared from the micellar solution, in the range of 0.3 wt.% of Triton X-100, exhibited much higher discharge capacities, as well as better cyclabilities in comparison with the commercial EMD sample known as TOSOH™. The superiority of the former EMD was further confirmed through electrochemical cyclic voltammetry and also electrochemical impedance spectroscopy (EIS). Modifications of electrolytic MnO_2, via mediations of different surfactants were perceived through changes in their compositions, crystal structures and morphologies. The characteristics of the produced materials were determined by thermogravimetric analysis (TGA), powder X-ray diffraction (XRD) and scanning electron microscopy (SEM).

Enhancements of electrochemical properties, observed for Triton X-100 modified EMD, could be attributed to a homogeneous current distribution with unique crystalline structure, based on the modified electrode/solution interface, through adsorbed surfactant layers. Moreover, the observed improvements appear connected to the enhanced film growth, with different degrees of mesoscopic organizations. Higher cycle performances, mechanical stabilities and the ease of production make this method excellent for being employed in a number of industrial applications.

Keywords: Surfactant; Electrodeposition; Manganese dioxide; Rechargeable alkaline batteries

1. Introduction

While the employment of manganese dioxide in lithium batteries is at embryonic stage, its usage in alkaline batteries dates back to about 40 years ago and it has been exploited in Leclanché batteries for over a century [1–4]. Even though, electrolytic manganese dioxide (EMD) has demonstrated a high electrochemical activity and environmental compatibility, there is still a profound desire to overcome its irreversibility [5–10]. Hence, the purpose of this study is to enhance the cycle life of rechargeable alkaline manganese dioxide–zinc batteries (RAM) by designing a highly porous network of manganese dioxide [11]. It is evident that such an objective might not be accomplished through delocalized electrosynthesis of EMD, where electrodeposition preferentially starts at the substrate surface inhomogeneities [12].

Beneficial effects of localizing heat through non-isothermal anode heating [13] on electrokinetics, have led us to use a relatively new technique with more efficiency in energy conversion, for the evaluation of EMD. Adsorption of

* Corresponding author. Tel.: +98 21 800 6631/801 1001; fax: +98 21 800 9730.
E-mail address: ghaemi_m@modares.ac.ir (M. Ghaemi).

0378-7753/$ – see front matter © 2004 Elsevier B.V. All rights reserved.
doi:10.1016/j.jpowsour.2004.10.004

surfactants at the electrode/solution interface [14] appeared to be an attractive, simple methodology to improve the electrochemical processes at the substrate/electrolyte interface. Though researches have been carried out on surface active agents in electrochemistry for more than six to seven decades, just a few classes of materials have been well studied so far for a modification process in the presence of surfactants [15]. Employment of surfactants in this work is a natural outgrowth of numerous and valuable articles on surface active agents. As proposed by Rusling, surfactant layers are formed on the electrode surface with well-defined microstructures and these could serve as templates for the electrochemical reactivity [16–18]. Based on liquid crystalline phases of highly concentrated surfactants (>30 wt.%), an electrolytic method is developed, for fabricating thin films with enhanced crystal growth, by Attard and coworkers [19–21]. The modified materials are expected to afford superior mass transport properties, through regular mesoporous networks as a result of modified growth on the surface of adsorbed organic surfactant layers. Consequently, such modifications affect the morphology, crystallinity, mechanical properties and hence electrochemical activity of materials [22].

We report in this work that EMD obtained from very dilute neutral surfactant solutions (<0.5 wt.%), has a much lower deterioration rate during redox cycling in comparison with commercial samples. The origin of this positive effect may be ascribed to a possible decrease of the extent of swelling or contraction upon redox cycling through apparently higher porosity and mechanical stability. Furthermore, the feature and interest of the dynamic and complex system of surfactants mediated route in production of novel electroactive materials are discussed and compared to those of conventional industrial methods, produced in the absence of surfactants.

2. Experimental

2.1. Material synthesis and preparations

Electro-oxidation of MnO_2 was performed at anodic current densities of $\leq$0.5 A dm^{-2} during 72 h using a laboratory scale electrolyzer. All EMD samples were prepared by adding different quantities of surfactants directly to the aqueous sulfuric acid (0.5 mol l^{-1}) electrolyte containing manganese sulfate (112 g l^{-1}). The anode was made of 6.5 cm diameter titanium cylinder of 12 cm height. The cathode, which was placed inside the inner compartment, consisted of a 4 cm diameter Pb cylinder of 10 cm height. The detailed descriptions of the cell construction and procedures can be found in our previous work [13].

The critical micelle concentration (cmc) values of Triton X-100 (abbreviated as TX-100, Merck), CTAB (Merck) and SDBS (Aldrich) is equal to 3.0×10^{-4} M (0.02 wt.%), 3×10^{-3} M (0.1 wt.%) and 1.2×10^{-3} M (0.04 wt.%), respectively [23–25]. Molecular structures of these surfactants are displayed in Fig. 1a.

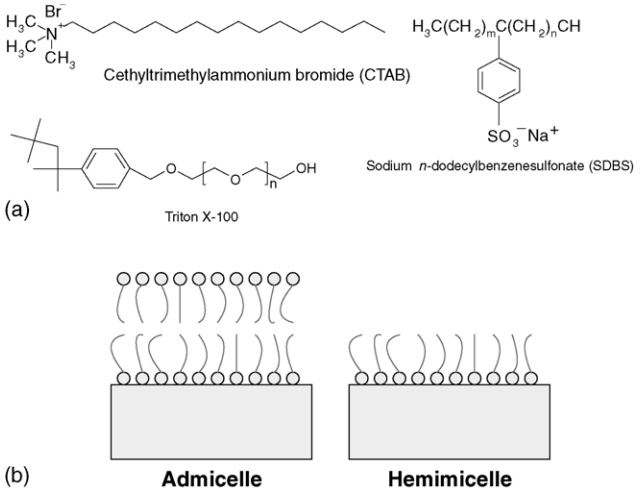

Fig. 1. (a) Molecular structures of surfactants; (b) different arrangement of surfactants at the electrode/solution interface.

Electrolyte solutions with TX-100 concentrations of 0.5, 1, 3, 10, 17, 23 and 35 times cmc value were prepared and the resulting EMD samples have been labeled as MDTX0.5, MDTX1, MDTX3, MDTX10, MDTX17, MDTX23 and MDTX35, respectively. The concentrations of CTAB in the electrolyte were 0.5, 1, 3, 17 and 35 times cmc and the resulting EMD samples have been labeled as MDCT0.5, MDCT1, MDCT3, MDCT17 and MDCT35, respectively.

The concentrations of SDBS in the electrolyte were 7, 12 and 23 times cmc and the resulting EMD samples have been labeled as MDSD7, MDSD12 and MDSD23, respectively. The sample MD0 was obtained through the same conditions but without addition of any surfactants in the preparation bath. The deposited EMD layer was mechanically removed, rinsed with distilled water and ground with a pestle and mortar. The EMD powder obtained was washed well and neutralized using 10% ammonia solution followed by sufficient distilled water until the washing solution reacted neutral. Subsequently, the samples were dried at 75 °C overnight and the product was then sieved using 100 μm mesh screen.

Since surface morphologies of samples could be affected by various dissimilar electrolysis parameters and/or the alteration of the bath composition during electrolysis, a short time electrosynthesis of 12 h was performed at a current density of $\leq$0.1 A dm^{-2}. Thin layers of EMDs were scraped off the anode, washed thoroughly with distilled water, and dried in air for further study of the surface morphology.

2.2. Charge/discharge cycling

The charge/discharge cycle performances of EMD samples were tested as the main cathodic component of RAM batteries. The constructions of these laboratory designed batteries were described previously [26]. The composite cathodes were prepared by mixing the EMD powder (90 wt.%), Graphite (Lonza KS 44, 9.5%) and carbon black (0.5%), and pressed at 6 t cm^{-2} for 6 min on a stainless steel plates

to form a cathode ring. Anode gels composed of 31 wt.%, 12N KOH solution, battery grade zinc powder (61.5%), MgO (2%), ZnO (3.4%), alfa cellulose (1%) and Starch (Farinex 273) (1.1%). Cycling experiments were performed using a computer-controlled battery-testing system. The first series of cells have been charged and discharged galvanostatically at a current density of 30 mA g^{-1} MnO_2 and the second series were discharged through a constant resistance and charged by voltage limited taper current (VLTC) method to 1.72 V. All cells were discharged to a cut-off voltage (COV) of 0.9 V. The discharge capacities were recorded and compared with standard reference cells made with industrial EMD (TOSOH Hellas, Greece) as well as MD0 up to 15 cycles.

2.3. Characterization, analysis and further electrochemical test procedures

Cyclic voltammetry (CV) experiments were performed in 9 M KOH, with the aid of Potentiostat/Galvanostat (EG&G 273A) instrument using a three-electrode arrangement of a working electrode, platinum wire auxiliary electrode and Hg/HgO reference electrode. The working electrode is composed of EMD/graphite powder mixture with a weight ratio of 2:98. This was mixed with sufficient 9 M KOH and pasted on a glassy carbon electrode (Ø 2 mm).

Electrochemical impedance spectroscopy (EIS) measurements were carried out with a working electrode prepared by thoroughly mixing EMD samples (90%) with graphite (9.5%) and carbon black (0.5%) in 9 M KOH. The mixture (0.4 g) was compressed at 7 t cm^{-2} into stainless steel strips as current collector to form a disc. EIS tests were then carried out in KOH 9 M, in the range of 100 kHz and 10 mHz, at open circuit voltage (OCV) and ±5 mV potential amplitude.

The surface morphology of the grown films was investigated by scanning electron microscopy (Philips XL 30). Thermal gravimetric analysis of EMD was carried out by means of PL-STA1500, at a ramp rate of 10 °C min^{-1}. Powder X-ray diffraction (XRD) patterns were recorded using a Philips Xpert diffractometer and Cu Kα radiation (λ = 0.15418 nm). Total organic carbon analysis (TOC) of EMD samples was done by means of Skalar CA 10, in order to determine the extent of the adsorption of organic species into EMDs.

3. Results and discussion

3.1. Kinetic aspects of EMD electrodeposition process in the presence and absence of surfactants

The electrodeposition of manganese dioxide in acidic aqueous solution is believed to be affected essentially by the following successive steps:

$$Mn_{sol}^{2+} \rightarrow Mn_{ads}^{3+} + e^- \quad (1)$$

$$2Mn_{ads}^{3+} \rightarrow Mn_{ads}^{4+} + Mn_{sol}^{2+} \quad (2)$$

Kinetics of the first step corresponds to the oxidation of Mn^{2+} at the growing surface of MnO_2 to produce Mn^{3+} and some related solid intermediates (like MnOOH, Mn_2O_3, etc.). Mn^{3+} is unstable in hot acidic solution and disproportionate slowly into Mn^{2+} and Mn^{4+}. The Mn^{2+} ions remain in the solution, whereas Mn^{4+} converts via a rather fast hydrolysis reaction to a solid MnO_2 deposit, which traps Mn^{3+} ions [27,28]. Bath temperature, pH, current density and other parameters control the percentage of Mn^{3+} and that of crystal defects namely De Wolff and microtwinning (Tw) [29–32]. De Wolff is a random structural defect, which corresponds to intergrowths of rutile-type structural units within the ramsdellite structure (Pr is the rutile concentration). Microtwinning was shown to be associated with the Mn^{4+} vacancies generated by oxygen evolution during MnO_2 electrodeposition [28]. Under high anodic current density, when Eq. (1) occurs too rapidly compared to Eq. (2), the anodic peak potential shifted to the values at which the EMD deposition is accompanied with more intense oxygen evolution and incompletely intermediate transitions. Under these circumstances, a second layer of Mn^{3+} and oxygen will form before the first Mn^{3+} layer complete its filling (Eq. (1)) and disproportionation (Eq. (2)) [33]. Consequently, the formation of a twin becomes energetically more favorable since the crystal would be filled with a Mn^{3+} or a vacancy instead of Mn^{4+}. EMDs prepared at very low current densities, exhibit both low microtwinning and low cation vacancy fractions. This is correlated to an increase of the O/Mn ratio and a higher density of EMD. Furthermore, the pH of the bulk solution is also an important parameter. Whatever the temperature, a pH increase seems to favor smaller Pr values [34]. Both defects can interrupt the structural homogeneity and proton diffusion pathway [35].

Adsorption of surface active agents on the interface may inhibit the rate of Eq. (1) in comparison with Eq. (2). Because of adsorption of surfactants at the active growth sites (e.g. twin boundaries) and on surface high points, much less adsorption will occur in the recesses and hence the material tends to be preferentially deposited in the recess [36]. In addition, the transport of electroactive species through a possible formation of patches on the interface, micropores and interparticle channels in the active material is harder, thus resulting in inhibition and lower current values [37].

The dependence of electron/ion transfer kinetics on the degree of coverage of the electrode by surfactants is mostly interpreted as the result of the mechanical blocking and/or electrostatic effects [38,39]. This could cause changes in the characteristics of the electric double layer and all other related phenomenon at the interface such as interfacial energy, dielectric constant, potential and current distribution that are associated with modifying of the crystal growth. For a regular crystal growth, the diffusivity of the adatoms in the pores with different sizes needs to be high, which requires high temperatures. Consequently, adatoms could be caught and incorporated by the next upward step rather than nucleation of new islands on top of existing ones [40].

The inhibition of surface diffusion of adatoms, which could even be the rate determining step, occurs also under conditions of higher anodic reaction rates (higher rate of Eq. (1) compared to Eq. (2)), leading to faster and increased nucleation [41].

However, it has been reported that in the presence of surfactants the surface diffusion of adatoms could be facilitated and thus the production of excess new crystal nuclei is suppressed [42]. Nucleation rate (J) and interfacial Gibbs energy change (ΔG) are related to interfacial surface tension change ($\Delta\sigma$) [41].

The tendency of surfactants to keep the interfacial surface tension over the growing electrode surface, results in organized position of adatoms on the proper site of the growing surface. This translates into formation of compact deposits, having large surface areas and narrow pore size distributions with enhanced adhesion to the substrate. Otherwise, the deposits are loose, and their adhesion is considerably worse. According to our experimental results, better adherence of MDTX17 sample on titanium was observed in comparison with other samples. This appears due to modified electrokinetics on the entire surface of the electrode which could affect the nature of MnO_2 crystal orientation [43].

Another aspect of decreasing surface tension is that the activation energy or surface temperature required to initiate gas/vapour bubble nucleation, could be reduced [44]. At low concentration of surfactants, large number of smaller gas bubbles could be generated which nucleate uniformly on the substrate surface and grow up rapidly. At higher surfactant concentrations, the increase in interfacial viscosity accompanied with difficulties of bubbles escape from interface [45]. Consequently, the rate of diffusivity and mass transfer is decreased, especially in the case of O_2-evolving electrodes. Therefore, decrease of limiting current could be expected as a result of gas hold-up, ohmic potential drop (IR) and electrode overvoltage leading to an irregular morphology, as observed for MDTX35 in our experimental conditions [46]. Careful monitoring of surfactant concentration and bath composition is therefore necessary to achieve good reproducibility in the electrosynthesis.

3.2. Influences of surfactants on electrosynthesis

The knowledge of structures and possible orientations of surfactants often helps to predict their corresponding reactivities and interactions [47]. Surfactants are actually molecules with single- or double-chain aliphatic, nonpolar regions and ionic or neutral polar head groups [48]. These amphiphilic molecules can adsorb and desorb at solid/solution interfaces depending on the applied potential ranges [49]. Below the critical micelle concentration (cmc), when coulombic interactions between head groups and surfaces are very strong, hemimicelles are formed (Fig. 1b). This is a surfactant layer with hydrocarbon chains facing the water [50].

At lower concentrations of surfactants, complex formation with dissolved species is also possible [51]. As the concentration of surfactants increases, different structural forms could be created in the diffusion layer of the electrode [38]. The surfactants adsorbed onto charged surfaces could arrange in bilayers called admicelles (Fig. 1b). This is a molecular layer with head groups down on the surface and a second layer with head groups facing the solution [51]. At higher concentrations of surfactants, the electrode surface may be less accessible to the water molecules and/or H^+ ions [52]. Ionic strength, pH, temperature and the nature of solid and solvent could affect the adsorption and transfer processes [53].

TX-100 molecules tend to be oriented with the phenyl ring toward the solution [54]. The presence of hydroxyl groups would strengthen the adsorbability toward the EMD electrode surface, forming an adsorbed surfactant layer, rendering the surface more hydrophobic. However, there is no reason to believe an inflexible arrangement of TX-100 molecules with the hydrophilic ends bonded to the electrode surface. At concentrations higher than cmc and/or certain synthesis parameters, surfactant arrangement may assume all possible conformations, including the interweaving of hydrophobic chains of adjacent molecules and the formation of admicelles [54].

TX-100 could act as a molecular spacer through the steric factor of the phenyl ring [47]. The structure functions as a path for Mn^{2+} ions facilitating uniform current distribution. Namely, a moiety of few ethylene oxide (EO) units in the film may mediate between manganese ions solvated in the electrolyte and oxide film [55]. The oxygen atoms in the polyoxyethylene group of TX-100 may attract the positive charge of Mn^{2+}, resulting in Mn^{2+}–TX-100 complexes. Transfer process through these types of complex formation, which are probably van der Waals in nature, could be affected through changes in surfactant concentrations. Sedahmed and coworkers have reported that, the rate of mass transfer decreases with increasing TX-100 concentration up to 0.3 wt.% and then remains almost constant with further increase in concentration [45]. The improved properties of MDTX17, produced in a bath containing around 0.3% TX-100, may be related to the effect of mass transfer on electrocrystallization process. The negative effect of TX-100 at concentrations >0.3%, could be ascribed to the increase in the interfacial viscosity and a decrease in diffusivity of the diffusion controlled electrooxidation of MnO_2.

In the positive potentials ranges, anionic species can be much more strongly adsorbed than cationic ones with their head groups at the surface. While CTAB may repel from the anode surface, anionic SDBS will be attracted to the anode surface, cover a part of this surface and hindering the access of manganese species to the electrode surface. However, ionic surfactants such as SDBS and CTAB could also form micelles (in solution) and admicelles at the interface, when the surfactant concentration is above the cmc This causes a charge reversal at the inner boundary of the diffuse layer accompanied with a change in the double layer characteristics and electrokinetics.

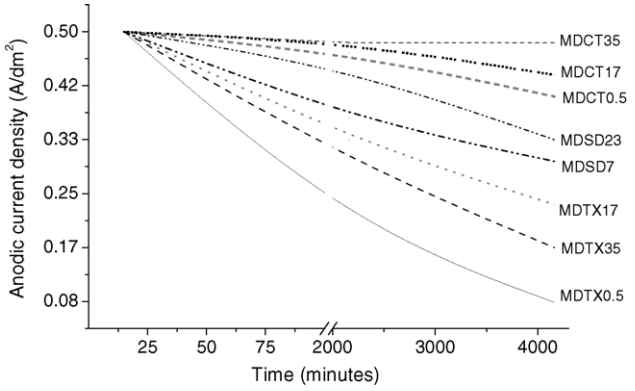

Fig. 2. Effect of the nature and concentrations of surfactants on the current loss during the electrolysis; initial current density = 0.5 A dm^{-2}, t = 4320 min.

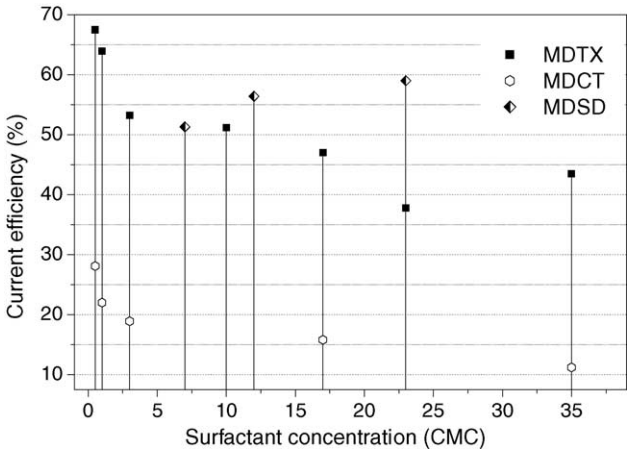

Fig. 3. Current efficiencies of various surfactant containing electrolyte solutions, during electrosynthesis of different MnO_2.

In the potential region of water decomposition, surfactants could be deactivated and oxidized by the action of intermediates of water discharge (e.g. oxygen radicals, especially the hydroxyl radicals and hydroxyl ions) [56]. In some experiments, especially those carried out with TX-100 concentration >0.2%, brown sticky organic compounds were observed during electrolysis, denoting that the surfactants had undergone some chemical changes due to electrolysis. According to TOC analysis, 1 mg C g^{-1} MnO_2 was detected in MDTX0.5, indicating that nearly all TX-100 molecules or its degradiated compounds are incorporated into the MDTX0.5 sample. The amount of carbon in MDTX35 and MDSD samples were negligible, whereas 1.7 and 0.5 mg C g^{-1} MnO_2 was measured for MDTX17 and MDCT3, respectively. Further detailed study is necessary to determine effects of various degradiated organic compounds to predict a relation between the TOC values and physico-chemical properties of EMD.

The mentioned complex effects of surfactants would influence the current conditions. The variation of current versus time was noted in order to collect information about the type of mechanism occurring during electrochemical processes. The current–time curves recorded during 72 h electrolysis showed that the current are suppressed on increasing concentrations of surfactants in a manner consistent with the less accessible area of the electrode available for the reaction (Fig. 2).

The influence of the surfactant concentration on the electrolysis product yield was also investigated. Adsorption of strongly adsorbable surfactants, such as TX-100, gives rise to an increase of hydrogen and oxygen overpotential. This is correlated to the promotion of charge-acceptance capability and increase of current efficiency indicating that all the current was consumed for the formation of MnO_2 [57]. In the case of ionic surfactants, especially CTAB, the yield was significantly lower probably due to water electrolysis (Fig. 3). The quantitative differences in current efficiencies between the TX-100 and CTAB micellar systems may be due to different interactions with free radicals formed during electrolysis, different structure and/or wettability formed by these surfactants as well as to their different degrees of electrochemical degradation of surfactants.

3.3. Scanning electron microscopy

Many investigations have shown that rechargeability, current efficiency and stability depend significantly on the electrode morphology. Surfactants strongly affect the morphology and crystal growth in association with a promotion of nucleation and current distribution [22]. In this regard, the structure of products is controlled through a balance of thermodynamic and kinetic forces within different inorganics, organics as well as inorganic/organic interactions [57]. Fig. 4 shows that the morphology of EMD deposits would be affected with a change in the surfactant composition. Addition of TX-100 below cmc, as was employed for the synthesis of MDTX0.5, does not change substantially the surface morphology of MD0 (Fig. 4a). These spherical shaped samples have filament-like protrusions at their surface. The morphology of MDSD12, observed just at higher magnification value of 10 000×, shows a distribution of various sizes of smaller particles. Each particle consists of not well developed needle-like crystallites loosely packed together (Fig. 4e).

Characteristic morphologies were observed for MDTX17 and MDCT3 samples (Fig. 4b and f). The surface of the latter consists of small needle-like fibers. The length of the fibers is several micrometers, while the diameter of the fibers is approximately 250 nm. The fibers are arranged roughly parallel to each other with excellent orientation and high surface area due to the high porosity. The rather rod-like crystals in MDCT3 are smaller and more perpendicular to the electrode surface compared to MDTX17. The surface of MDTX35 (Fig. 4d) shows dramatic changes in shape and crystallinity with rather amorphous morphology. This suggests that TX-100, at concentrations > ∼0.5%, cannot coordinate electroactive species and fail to form organized surfactant-inorganic aggregates on the electrode surface.

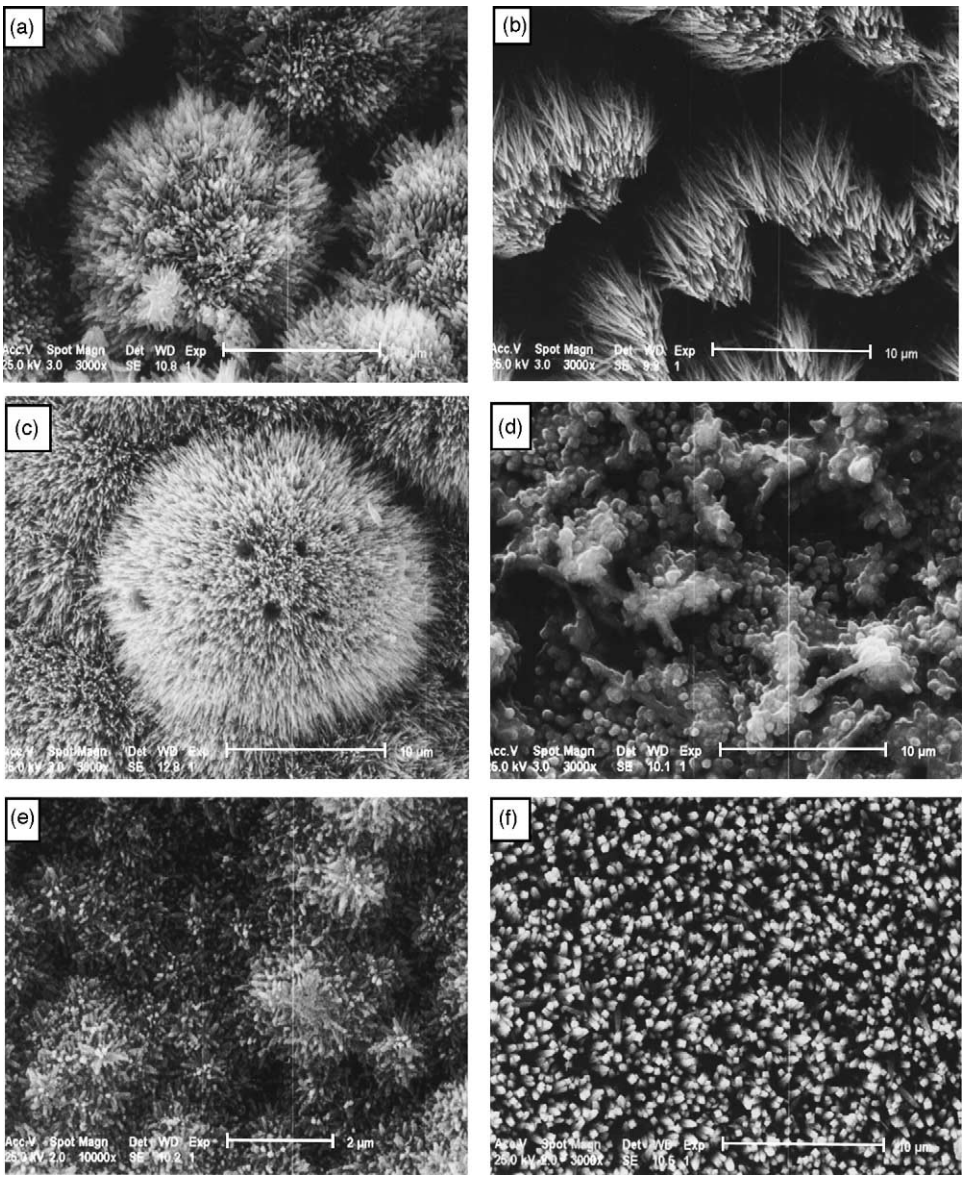

Fig. 4. Scanning electron micrographs of the surfaces of: (a) MDTX0.5; (b) MDTX17; (c) MDTX23; (d) MDTX35; (e) MDSD12; (f) MDCT3. Samples are coated with approximately 5 nm of gold.

3.4. Electrochemical performances

Fig. 5 plots the relation between cumulative capacities and cycle numbers in constant current and Fig. 6a and b in constant resistance mode. The capacities of the first-cycle discharge, of all EMD samples are comparable in the latter mode. For MD0 and all other MDCT samples, except MDCT3, rather poor capacities in the early cycles through constant current mode were observed. By increasing surfactant concentration, there was an alteration in the cycle behavior and the optimum was reached for MDTX17 (Fig. 6b). Discharge performance of the latter was essentially very similar to that reported for the best modified EMD material prepared through non-isothermal electrode heating [13]. Following factors may be the main reasons for the enhancement of the cycle-life. The presence of TX-100 could strengthen the skeleton of the EMD and prevents the capacity loss. Secondly, large surface area of the needle-like crystals decreases the solid-state diffusion path length of protons and electrons into and out of the bulk of MnO_2 films [5]. Therefore, more facilitated volume pulsations of EMD during charge/discharge cycling, and consequently an increase of both discharge capacity and coulomb efficiency could be expected. Such features appear particularly important from the viewpoint of conductance, as these needles should allow a much better connection of MnO_2 with graphite, explaining the higher cycle performance of the corresponding cells [58]. In spite of modified crystal structure and negative influence of α-MnO_2 (Fig. 7) on the rechargeability of MDCT3, its cycle behavior is better than MD0 and comparable to that of TOSOH (Fig. 5). This could

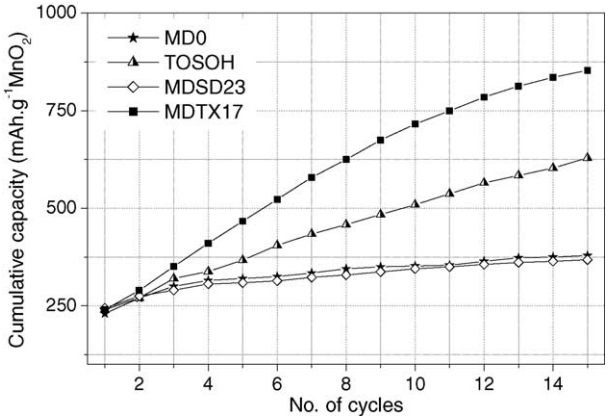

Fig. 5. Cumulative capacities of test batteries containing MDSD23 in comparison with MD0, TOSOH and MDTX17. Constant current charge and discharge of 30 mA g^{-1} MnO_2 was employed; cut-off voltage (COV) = 0.9 V; final voltage = 1.72 V.

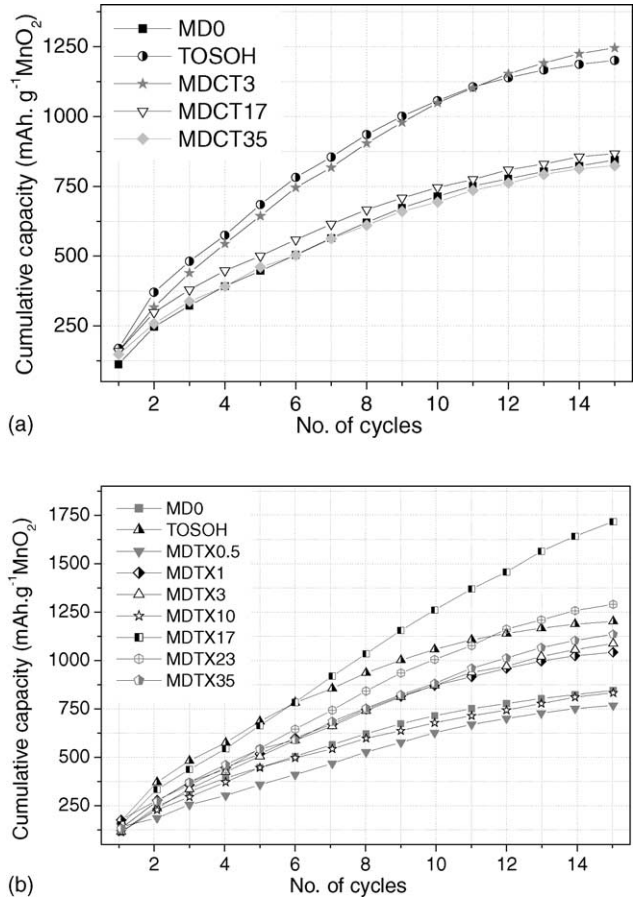

Fig. 6. (a) Cumulative capacities of test batteries containing MDCT samples in comparison with MD0 and TOSOH. Cells were discharged at constant resistance of $R = 33\,\Omega\,g^{-1}$ MnO_2 to 0.9 V and charged by voltage limited taper current (VLTC) method to 1.72 V. (b) Cumulative capacities of test batteries containing MDTX samples in comparison with MD0 and TOSOH. Cells were discharged at constant resistance of $R = 33\,\Omega\,g^{-1}MnO_2$ to 0.9 V and charged by voltage limited taper current (VLTC) method to 1.72 V.

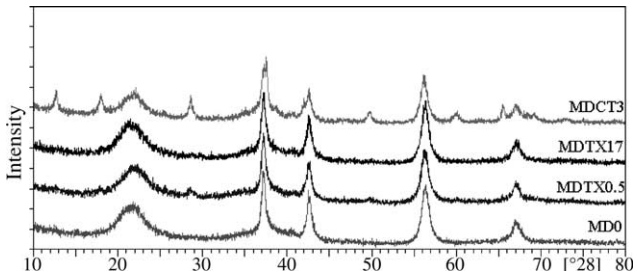

Fig. 7. Powder XRD patterns of MD0, MDTX0.5, MDTX17 and MDCT3.

be explained by the fact that, in the compressed cathode ring, loosing of electroactive species maybe partly compensated through a better connection of MDCT3 to graphite particles, owing to the special morphology. The released electroactive species could be adsorbed and accumulated on the surface of graphite and contribute to further redox process in batteries.

As shown in Fig. 5, MDSD23 and all other MDSD samples (not shown in the figure) have low discharge capacities. Thus, further experiments are carried out with cationic and non-ionic surfactants.

3.5. XRD

Fig. 7 shows that XRD pattern of MDTX17 was very similar to that of MD0. Both deposits have the same γ-MnO_2 crystal structure with no differences in the peak positions and peak intensities. In addition to the pure phases, mixtures were also obtained for MDTX0.5, which exhibits a certain amount of pyrolusite (β-MnO_2 as Pr defect). This could be observed by a shift of the (1 1 0) line at $2\theta \cong 22^\circ$ to higher angle compared to the position of the 1 1 0 line in MD0 [59]. Additionally, the weak reflection at 28.5° in 2θ confirms also a higher content of pyrolusite impurities in MDTX0.5 [32]. The lower capacity of the battery with MDTX0.5 cathode could be related to the rutile type lattice distortion and narrower diffusion path of β-MnO_2.

A two phased mixed crystals of α- and γ-MnO_2 obtained for MDCT3 displays a possibly phase separated crystals. Despite an enhanced morphology in MDCT3 in comparison with MD0 (Fig. 5), the presence of α-MnO_2 may be the main reason for its lower electrochemical cycle performances compared to MDTX17.

3.6. Cyclic voltammetry

The characteristic CV shapes of different EMD samples were maintained after 3 cycles within a potential window of −0.85 to +0.4 V versus Hg/HgO electrode (Fig. 8).

The reduction process occurs in three main steps observed in the range of 0–0.4 V [60]. The first step is related to the proton insertion in the channels of ramsdellite chains and the second one assigned to H^+/e^- insertion into the pyrolusite blocks. A third peak between −0.4 and −0.6 V can be followed by Mn^{2+} dissolution to form pyrochroite $Mn(OH)_2$. The corresponding oxidation is revealed in the voltammo-

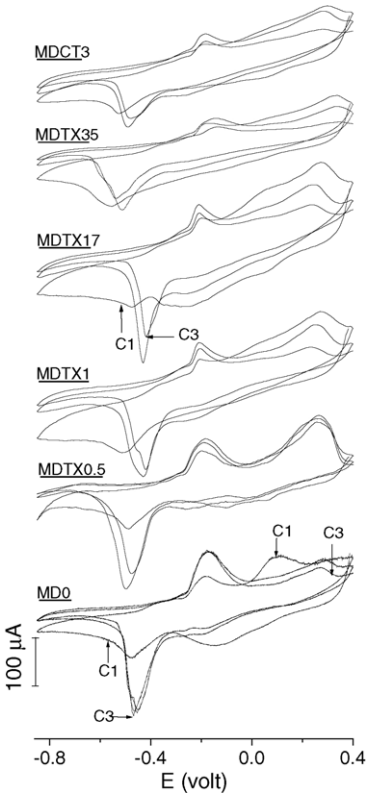

Fig. 8. CV responses of MD0, MDTX0.5, MDTX1, MDTX17, MDTX35, MDCT3 in 9 M KOH recorded at 0.25 mV s^{-1} carried out on glassy carbon electrode (Ø 2 mm) at 25 °C, reference electrode (Hg/HgO), auxiliary electrode (Pt).

gram by a peak centered roughly near −0.25 V, followed by a shoulder beginning near 0 V. This oxidation leads to the formation of δ-MnO_2. As a consequence, the behavior observed during the subsequent discharge is different and results in a lower capacity [61].

Because of the formation of an insulating intermediate and loosing of electroactive species (Mn^{3+}, MnOOH), the current may be suppressed. This is also observed for MD0 as confirmed by Nijjer et al. [62]. A decrease in overpotential for the reduction of Mn^{3+} to Mn^{2+} could be due to larger quantities of Mn^{3+} formed during the first cycle. The broad and large second cathodic peaks observed in MD0 and MDTX0.5 is in accordance to this assumption. Additionally, a strong current suppression of the first cathode reduction in the first scan seems to be due to a higher passivity of MDTX0.5. Additionally, higher warburg impedance observed in the latter proves a lower diffusion rate as confirmed by EIS measurements (Chapter 3.7).

MDTX17 showed the best performance from the electrochemical point of view. The sharpness of peaks in the voltammogram indicates a fast charge transfer, facilitated by highly accessible pore structure, in which the diffusion of ions is rapid and unhindered [40]. The lower peak separation signifies an increase in the reversibility of the electro-chemical redox processes.

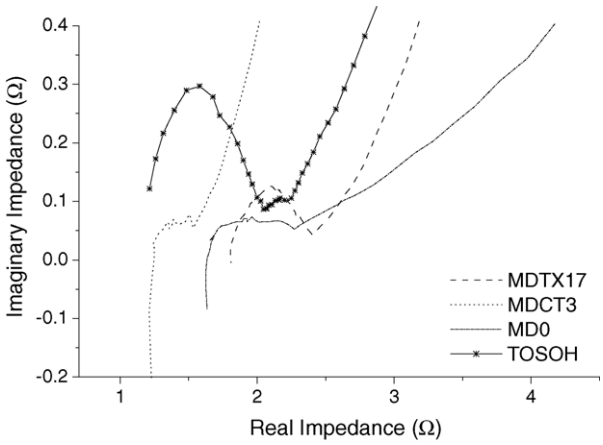

Fig. 9. Nyquist plots for MD samples: 9 M KOH, reference electrode (Hg/HgO), auxiliary electrode (Pt), working electrode area 1 cm^2, frequency range 100 kHz to 10 mHz.

In the range of anodic potentials, the first oxidation peak observed for MDTX17 and MDTX1 is shifted to more negative, whereas for MDTX35 it is shifted to more positive potentials. The higher peak separation in the latter indicates a lowering of the reversibility and a difficult charge and mass transfer kinetics. The reduction of the peak intensities in MDCT3 could be attributed to some extent to the presence of α-MnO_2, within a likely loose structure and a possible loss of electroactive species.

3.7. Electrochemical impedance investigation

Nyquist diagrams for EMDs are presented in Fig. 9. The simulation of experimental and calculated parameters was evaluated using Boukamp's program. The relation of R_{ct} (charge transfer resistance) and the electrochemical exchange current i_0, can be presented as follows [63]:

$$R_{ct} = RT/nFi_0 \quad (4)$$

where n is the number of exchanged electrons and F is the Faraday constant. According to the experimental observations, an equivalent electrical circuit is proposed, based on a physical picture of the EMD electrode (Fig. 10) (Table 1). This permits the use of a constant phase element (CPE) in equivalent circuit [64]:

$$Z_{CPE} = \delta\omega^{-n}\{\cos(n\pi/2) - j\sin(n\pi/2)\} \quad 0 < n < 1 \quad (5)$$

where δ and n are the CPE pre-factor and exponent, respectively. The terms R, Z_{CPE1} and Z_{CPE2} in the circuit, are

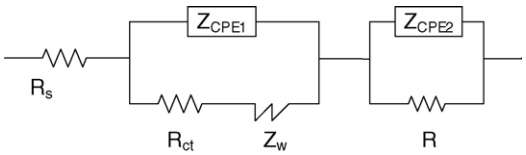

Fig. 10. Suggested equivalent circuit.

Table 1
Calculated equivalent circuit parameters of MD0 and MDTX17

	R_s (Ω)	Z_{CPE1} (Ω^{-1})	n_1	R_{ct} (Ω)	Z_w (Ω)	Z_{CPE2} (Ω^{-1})	n_2	R (Ω)
MDTX17	1.75	0.75	0.3	0.48	0.1	800	0.6	0.6
MD0	1.65	0.5	0.3	0.75	0.22	1000	0.6	0.4

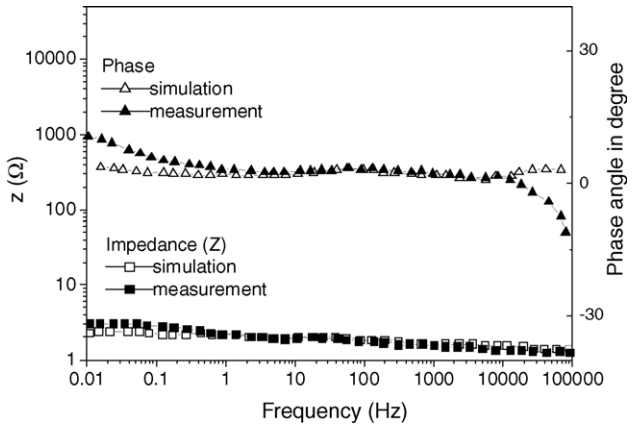

Fig. 11. Comparison between predicted and experimental impedance data of MDTX17, simulated by BOUKAMP 1988.

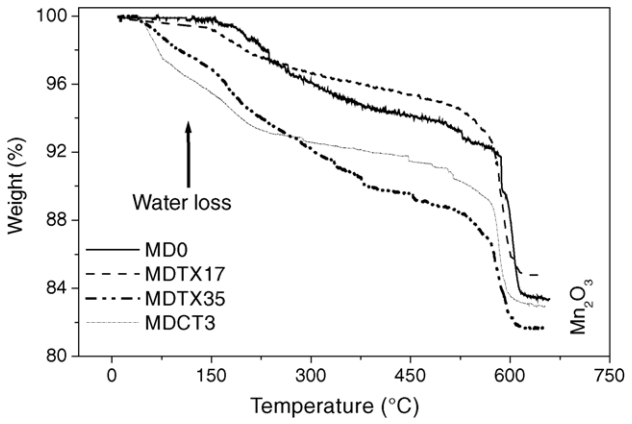

Fig. 12. TGA curves of MDTX, MDCT and MD0 samples between *RT* and 700 °C at 10 °C min^{-1}.

appeared because of the variable roughness and porosity of the EMD electrode. The fitted data follows in a satisfactory fashion the experimentally obtained impedance responses, thus confirming the validity of the simulation (Fig. 11).

Positive effects of TX-100 and CTAB on the electrode kinetics are reflected on impedance data as shown in Table 2. R_{ct} decreased in the case of MDTX0.5–MDTX23 samples as well as for MDCT3, due to the enhanced interfacial phenomena. The relatively lower R_{ct}, of MDTX samples indicates a higher I_0 and thus a faster kinetics and higher electrochemical reversibility in comparison with conventional TOSOH and MD0. However, the most relevant difference remains between the values of warburg impedance Z_w, which is due to porous nature of EMD and diffusion within interior of the solid structure. The lower Z_w of MDTX17 and MDCT3 prove to have a shorter diffusion path length, with enhanced proton diffusion kinetics into and out of bulk materials.

3.8. Thermogravimetric analysis

Water content in manganese dioxide is known to affect the electrochemical reactivity and thermodynamic stability of various MnO_2 phases, as it causes a variation in crystal lattice and a consequent variation in electrical conductivity and electrode potential [5]. Release of loosely bonded water between 25 and 200 °C, corresponds to an endothermic process [65]. The weight loss of MDTX17 is higher in this region in comparison with MD0, facilitated probably through a larger surface area (Fig. 12).

A second weight loss and two endothermic processes are then observed between 200 and 500 °C corresponds to the simultaneous complete oxidation of manganese II to the IV state (for the incompletely oxidized samples) and the release of more strongly bound water [34]. The weight loss during the second step is substantially lower for MDTX17 than for other samples.

According to Ruetschi, losses corresponding to these two types of structural water, i.e. H_2O groups associated with the presence of cation vacancies are observed at ca. 200 and 300 °C, respectively. It appears that for the first one (between ca. 200 and 250 °C) the weight loss is always in fair agreement with the amount of structural water, corresponding to the H_2O groups associated with the presence of cation vacancies. Endothermal weight loss at 480–560 °C corresponds to Mn_2O_3 formation.

The stronger water release in the early stage of heating for MNTX35 and MNCT3 could be attributed to a loose structure and higher amount of interlayer water molecules, the release of which could cause a gradually break down of EMD during cycling.

Table 2
Charge transfer resistance and warburg impedance of MD0, TOSOH, MDCT3 and all MDTX samples

Variable	MDTX0.5	MDTX1	MDTX3	MDTX10	MDTX17	MDTX23	MDTX35	MDCT3	MD0	TOSOH
R_{ct} (Ω)	0.97	0.67	0.47	0.41	0.48	0.34	0.59	0.31	0.75	0.78
Z_w (Ω)	0.23	0.17	0.15	0.13	0.10	0.12	0.13	0.11	0.22	0.30

4. Conclusion

In addition to the main parameters employed for synthesis of EMD, one can control its type and structure in the presence of surface active agents in the electrolyte solution. Our results indicated that the pure laboratory oxide obtained under similar conditions but in the absence of surfactants, is unfavorable for use in RAM batteries.

Modification of EMD electrode with neutral surfactants results in a better discharge performance and lower degradation rate. Whereas CTAB slightly promotes the charge/discharge cycle behavior of EMD, SDBS inhibits this process under our experimental conditions. The major parameter, toward enhanced electrochemical activities of the optimized sample MDTX17 is related to the facilitated diffusivity of electroactive ions and a regular crystal growth with enhanced needle like morphology. This may affect the penetration of electrolyte into micropores and ultimately proton mobility within the oxide lattice and increased electrical conductivity [65,5]. Through surfactant mediated synthesis of EMD it is also possible to obtain intimate mixtures of various crystal structures, such as interconnected α/γ-MnO_2.

Attempts to synthesize other electroactive materials like PbO_2, at TX-100 concentrations $\leq$0.35 wt.%, in the bath containing nitric acid and lead nitrate at bath temperatures $\leq$100 °C, enhanced a higher crystallinity and structural hardness of the material obtained. A number of our preliminary data suggest that the modified EMD samples, synthesized in the presence of surfactants, have a high lithium insertion capacity.

The new approach demonstrated in this study is inexpensive, reproducible, and potentially versatile for the fabrication of electroactive materials. The findings of this work are in initial stages and more detailed experiments should be conducted to further enhance the active mass utilization through a better morphological and microstructural control.

Acknowledgements

The partial support of this research by NIRU Batteries Mfg. Co. Ltd. is gratefully acknowledged.

References

[1] S. Bodoardo, N. Penazzi, P. Spinelli, M. Arrabito, J. Power Sources 94 (2001) 194.
[2] T.W. Farrell, C.P. Please, D.L.S. Mc Elwain, D.A.J. Swinkels, J. Electrochem. Soc. 147 (11) (2000) 4034.
[3] R. Ekern, J.L. Rose, M.E. Armacanqui, J. Power Sources 70 (1) (1998) 133.
[4] R. Ekern, M.E. Armacanqui, J.L. Rose, J. Power Sources 70 (1) (1998) 167.
[5] S.C. Pang, M.A. Anderson, T.W. Chapman, J. Electrochem. Soc. 147 (2) (2000) 444.
[6] J.P. Rethinaraj, S. Visvanathan, J. Power Sources 42 (1993) 335.
[7] C.-C. Yang, S.-J. Lin, J. Power Sources 4913 (2002) 1.
[8] Y. Shen, K. Kordesch, J. Power Sources 87 (1–2) (2000) 162.
[9] Y. Sharma, M. Aziz, J. Yusof, K. Kordesch, J. Power Sources 94 (2001) 129.
[10] W. Jantscher, L. Binder, D.A. Fiedler, R. Andreaus, K. Kordesch, J. Power Sources 79 (1999) 9.
[11] P. Liu, S.H. Lee, C.E. Tracy, J.A. Turner, J.R. Pitts, S.K. Deb, Solid State Ionics 165 (2003) 223.
[12] E. Budevski, G. Staikov, W.J. Lorenz, Electrochim. Acta 45 (2002) 2559.
[13] M. Ghaemi, R.K. Ghavami, L. Khosravi-Fard, M.Z. Kassaee, J. Power Sources 125 (2004) 256.
[14] J.F. Rusling, D.J. Howe, Inorg. Chem. Acta 226 (1994) 159.
[15] R. Vittal, H. Gomathi, J. Phys. Chem. B 106 (2002) 10135.
[16] J.F. Rusling, Acc. Chem. Res. 24 (1991) 75.
[17] J.F. Rusling, Micropor. Mater. 3 (1994) 1.
[18] J.F. Rusling, Colloids Surf. 81 (1997) 123.
[19] G.S. Attard, P.N. Bartlett, N.R.B. Coleman, J.M. Elliott, J.R. Owen, J.H. Wang, Science 278 (1997) 838.
[20] I. Nandhakumar, J.M. Elliot, G.S. Attard, Chem. Mater. 13 (2001) 3840.
[21] T. Gabriel, I.S. Nandhakumar, G.S. Attard, Electrochem. Commun. 4 (2002) 610.
[22] J.O. Besenhard, J. Gürtler, P. Komenda, A. Paxions, J. Power Sources 20 (1987) 257.
[23] J. Zhang, P.R. Unwin, J. Electroanal. Chem. 494 (2000) 47.
[24] J. Epstein, J.J. Kaminski, N. Bodor, R. Enever, J. Sowa, T. Higuchi, J. Org. Chem. 43 (14) (1978) 2816.
[25] I.S. Chronakis, P. Alexandridis, Macromolecules 34 (2001) 5005.
[26] M. Ghaemi, Z. Biglari, L. Binder, J. Power Sources 102 (2001) 29.
[27] B. Prélot, C. Poinsignon, F. Thomas, E. Schouller, F. Villiéras, J. Colloid Interface Sci. 257 (2003) 77.
[28] B. Prélot, F. Villiéras, M. Pelletier, A. Razafitianamaharavo, F. Thomas, C. Poinsignon, J. Colloid Interface Sci. 264 (2003) 343.
[29] J.-R. Hill, C.M. Freeman, M.H. Rossouw, J. Solid State Chem. 177 (2004) 165.
[30] M. Arrabito, S. Bodoardo, N. Penazzi, S. Panero, P. Reale, B. Scrosati, Y. Wang, X. Guo, S.G. Greenbaum, J. Power Sources 97-98 (2001) 478.
[31] St. Rashkov, N. Atanasov, Electrodeposition Surf. Treat. 3 (1975) 105.
[32] Y. Paik, J.P. Osegovic, F. Wang, W. Bowden, C.P. Grey, J. Am. Chem. Soc. 123 (2001) 9367.
[33] S. Rodrigues, N. Munichandraiah, A.K. Shukla, J. Appl. Electrochem. 28 (1998) 1235.
[34] A. Le Gal La Salle, S. Sarciaux, A. Verbaere, Y. Piffard, D. Guyomard, J. Electrochem. Soc. 147 (3) (2000) 945.
[35] R.P. Williams, D.A.J. Swinkels, M. Maeder, Trends Anal., Chem. 9 (9) (1990) 303.
[36] K. Boto, Electrodeposition Surf. Treat. 3 (1975) 77.
[37] L.A.H. MacLean, F.L. Tye, J. Mater. Chem. 11 (2001) 891.
[38] Z. Kozarac, S. Nikolić, I. Ružić, B. Ćosović, J. Electroanal. Chem. 137 (1982) 279.
[39] I. Felhősi, J. Telegdi, G. Pálinkás, E. Kálmán, Electrochim. Acta 47 (2002) 2335.
[40] E. Bertel, N. Memmel, Appl. Phys. A 63 (1996) 523.
[41] M.M. Jakšić, J. Electroanal. Chem. 242 (1998) 21.
[42] Y. Matsumoto, M. Noguchi, T. Matsunaga, J. Phys. Chem. B 103 (1999) 7190.
[43] H. Luo, J. Zhang, Y. Yan, Chem. Mater. 15 (2003) 3769.
[44] D.S. Wen, B.X. Wang, Int. J. Heat Mass Transfer 45 (2002) 1739.
[45] A.A. Mobarak, M.S.E. Abdo, M.S.M. Hassan, G.H. Sedahmed, J. Appl. Electrochem. 30 (2000) 1269.
[46] J.F. Rusling, Z. Wang, A. Owlia, Colloid Surf. 48 (1990) 173.
[47] P. Matejka, B. Vlckova, J. Vohlidal, J. Phys. Chem. 96 (1992) 1361.
[48] R. Foucault, R.L. Birke, J.R. Lombardi, Langmuir 19 (2003) 8818.
[49] L. Ndiaye, P. Cowache, M. Cadene, D. Lincot, J. Vedel, Thin Solid Films 224 (1993) 227.

[50] J.F. Rusling, D.J. Howe, Inorg. Chim. Acta 226 (1994) 159.
[51] F.J. Srydlowskl, D.L. Dunmire, E.E. Peck, R.L. Eggers, W.R. Matson, Anal. Chem. 53 (2) (1981).
[52] G. Juhel, B. Beden, C. Lamy, J.M. Leger, R. Vignaud, Electrochim. Acta 35 (2) (1990) 479.
[53] H.S. Posselt, F.J. Anderson, W.J. Weber, J. Curr. Res. 2 (1968) 1087.
[54] B. Factor, B. Muegge, S. Workman, E. Bolton, J. Bos, M. Richter, Anal. Chem. 73 (2001) 4621.
[55] K. Naoi, M. Mori, M. Inoue, T. Wakabayashi, K. Yamauchi, J. Electrochem. Soc. 147 (3) (2000) 813.
[56] G. Lissens, J. Pieters, M. Verhaege, L. Pinoy, W. Verstraete, Electrochim. Acta 48 (2003) 1655.
[57] Y.Z. Khimyak, J. Klinowski, J. Mater. Chem. 10 (2000) 1847.
[58] M.A. Humbert, Ph. Biensan, M. Broussely, J. Power Sources 43–44 (1993) 681.
[59] L.I. Hill, A. Verbaere, D. Guyomard, J. Power Sources 119–121 (2003) 226.
[60] Z. Rogulski, H. Siwek, I. Paleska, A. Czerwiński, J. Electroanal. Chem. 543 (2003) 175.
[61] S. Jouanneau, A. Le Gal La Salle, D. Guyomard, Electrochim. Acta 48 (2002) 11.
[62] S. Nijjer, J. Thonstad, G.M. Haarberg, Electrochim. Acta 46 (2000) 395.
[63] S.W. Donne, J.H. Kennedy, J. Appl. Electrochem. 34 (2004) 159.
[64] S.W. Donne, J.H. Kennedy, J. Appl. Electrochem. 34 (2004) 477.
[65] W. Cheng, E. Baudrin, B. Dunn, J.I. Zink, J. Mater. Chem. 11 (2001) 92.